7
Surface Forces and Emulsion Stability

Per M. Claesson, Eva Blomberg, and Evgeni Poptoshev
Royal Institute of Technology, Stockholm, Sweden

I. INTRODUCTION

Emulsions are dispersions of one liquid in another liquid, most commonly water-in-oil or oil-in-water. The total interfacial area in an emulsion is very large, and because the interfacial area is associated with a positive free energy (the interfacial tension), the emulsion system is thermodynamically unstable. Nevertheless, it is possible to make emulsions with an excellent long-term stability. This requires the use of emulsifiers that accumulate at the oil–water interface and create an energy barrier toward flocculation and coalescence. The emulsifiers can be ionic, zwitterionic, or nonionic surfactants, proteins, amphiphilic polymers, or combinations of polymers and surfactants. The structure of the adsorbed layer at the water–oil interface may be rather complex, involving several species adsorbed directly to the interface as well as other species adsorbing on top of the first layer.

The first question one may ask is if an oil-in-water emulsion or a water-in-oil emulsion is formed then the two solvents are dispersed into each other with the use of a given emulsifier. There are several empirical roles addressing this problem. The first is due to Bancroft (1), who stated that if the emulsifier is most soluble in the water phase, then an oil-in-water emulsion will be formed. A water-in-oil emulsion will be obtained when the reverse is true. The HLB (hydrophilic–lipophilic balance) concept is used for describing the nature of the surfactant. It was first introduced by Griffin (2) and later extended by Davies (3). Hydrophobic emulsifiers having a low HLB number, say below 6, are predicted to be suitable for forming

water-in-oil emulsions, whereas more hydrophilic emulsifiers with high HLB values, above about 10, are suggested to be suitable for forming oil-in-water emulsions. The HLB value can easily be calculated from the structure of the emulsifier (3). An HLB value has also been assigned for most common oils. It is defined as the HLB number of the emulsifier in a homologous series that produces the most stable oil-in-water emulsion. A nonpolar oil is found to have a lower HLB number than a polar oil. Hence, the choice of emulsifier has to be adjusted to the type of oil that is to be emulsified.

The use of an HLB value for nonionic emulsifiers of the oligo (ethylene oxide) type has its drawbacks because their properties are strongly temperature dependent. This is clearly seen in three-component oil–water–surfactant phase diagrams. At low temperatures, microemulsions of oil droplets in water (Winsor I) are formed. In a small temperature interval, bicontinuous microemulsions (Winsor III) are stable, followed at higher temperatures by a microemulsion consisting of water droplets in oil (Winsor II). These transitions are due to a change in the spontaneous monolayer curvature from positive at low temperatures to negative at high temperatures. This behavior is closely mimicked by the thermodynamically unstable (macro)emulsions, and it is common to describe these emulsions in terms of the phase-inversion temperature (PIT). Below the PIT, the emulsion is of the oil-in-water type, whereas above the PIT, it is of the water-in-oil type. Very close to the PIT, no stable (macro)emulsions can be formed. It has been argued that this change in behavior, as for the microemulsions, is due to the change in spontaneous curvature of such surfactant films at the oil–water interface, particularly the ease with which hole formation leading to coalescence occurs (4). Note that the PIT depends not only on the nature of the emulsifier but also on the type of oil used, which often can be explained by the degree of oil penetration into the emulsifier film.

When two droplets approach each other, they will interact with hydrodynamic forces and with surface forces of molecular origin. Finally, when the droplets are close enough, they may coalesce and form one larger droplet. An emulsion will have a long-term stability if the droplets are prevented from coming close to each other by strong repulsive forces and if they are prevented from coalescing even when they are close to each other. However, in this case also, a slow destabilization due to Ostwald ripening will occur.

II. INTERACTIONS AND HOLE FORMATION

In this section, we will give a short overview of hydrodynamic and surface forces as well as hole formation leading to coalescence. References will be provided for the reader who wants to delve further into these subjects.

A. Hydrodynamic Interactions

When liquid drains from the gap between two approaching spherical emulsion droplets of equal size, a hydrodynamic force resulting from viscous dissipation is produced. As long as the surfaces do not deform (i.e., small forces) and the liquid next to the surface is stationary (no slip condition, see next page) the hydrodynamic force is given by (5).

$$F = -\frac{3\pi\mu R^2}{2D}\frac{dD}{dt} \tag{1}$$

where R is the radius of the spheres, μ is the viscosity of the draining liquid, D is the separation between the spheres, and t is the time. This equation describes the hydrodynamic interaction when the droplets are far apart and do not interact with each other very strongly. However, as soon as the interaction between the surfaces is sufficiently large, the emulsion droplets will deform and Eq. (1) is no longer valid.

In concentrated emulsions, we meet another extreme case. A thin planar liquid film now separates the emulsion droplets, and they may change their shape from spherical to polyhedral (6). In this case, the liquid drains out of the flat part of the film owing to the capillary suction pressure. The outflow of liquid between rigid parallel disks was considered by Reynolds (7,8) who found that the pressure varied with the radial distance from the center of the disk as

$$P = P_0 + \frac{3\mu}{D^3}(r_0^2 - r^2)V_R \tag{2}$$

where P is the pressure at a distance r from the center, r_0 is the radius of the plate, P_0 is the hydrostatic pressure, which equals the total pressure at the edge of the contact, (i.e., at $r = r_0$, and V_R is the rate of approach (i.e., $-dD/dt$).

The repulsive hydrodynamic force acting on the plates is obtained by integrating over the plate area and subtracting the hydrostatic pressure contribution:

$$\begin{aligned} F &= 2\pi\int_0^{r_0}(P - P_0)r\,dr = 2\pi\int_0^{r_0}\left[\frac{3\mu}{D^3}(r_0^2 - r^2)V_r\right]r\,dr \\ &= \frac{3\pi r_0^4\mu V_R}{2D^3} \end{aligned} \tag{3}$$

The average excess pressure (which equals the capillary pressure) between circular plates can be expressed as

$$\bar{P} = \frac{F}{\pi r_0^2} \tag{4}$$

Hence, we obtain the well-known Reynolds equation

$$V_R = -\frac{dD}{dt} = \frac{2D^3\bar{P}}{3\mu r_0^2} \tag{5}$$

We immediately see that the film-thinning rate is reduced, and thus the emulsion stability increased, by an increase in bulk viscosity. In the case in which the liquid film is so thin that surface forces no longer can be neglected, the capillary pressure term in the Reynolds equation should be replaced by the total driving force (ΔP) for the thinning. This is equal to the difference between the capillary pressure and the disjoining pressure (Π) due to the surface forces acting between the emulsion droplet surfaces: $\Delta P = (\bar{P} - \Pi)$. Clearly, a positive disjoining pressure (i.e., a repulsive force) reduces the driving force for film thinning and thus the drainage rate.

Experimentally determined rates of thinning do not always agree with the predictions of the Reynolds model. For foam films stabilized by an anionic surfactant, sodium dodecyl sulfate (9,10), it has been shown that typical thinning rates exhibited a much weaker dependence on the film radius ($r^{-0.8-0.9}$) than the predicted r^{-2} dependence. To obtain an understanding for why the Reynolds theory of thinning does not always agree with experimental results, it is worthwhile to consider two assumptions made when arriving at Eq. (5). First the result is valid only under "no-slip" conditions (i.e., the velocity of the liquid at the film interface is assumed to be zero). This is the case when the drainage takes place between solid hydrophilic surfaces. In contrast, only the adsorbed emulsifier layer provides the surface rigidity in foam and emulsion films, and it is not obvious that the no-slip condition is fulfilled. The drainage rate would be larger than predicted by Eq. (5) if this condition was not valid. Jeelani and Hartland (11), who calculated the liquid velocity at the interfaces of emulsion films for numerous systems studied experimentally, addressed this point. They showed that even at a low surfactant concentration, the liquid mobility at the interface is dramatically reduced by the adsorbed surfactant. Hence, it is plausible that when the adsoption density of the emulsifier is large (nearly saturated monolayers), the surface viscosity is high enough to validate the no-slip condition. It has been pointed out that a nonzero liquid viscosity at the interface is not expected to have an influence on the functional dependence of the drainage rates on the film radius (9). Hence, the deviations found experimentally have to have another origin.

A second assumption made when arriving at Eq. (5) is that the drainage takes place between parallel surfaces. Experimental studies on liquid films (9,10) have shown that during the thinning process, it is common that nonuniform films are formed which have a thicker region, a dimple, in the center. For larger films, even more complicated, multidimpled profiles have been found. Calculating the drainage rate for interfaces with such a complex shape is far from easy. However, recently Manev et al. (9) proposed a model for the drainage between nonparallel, immobile surfaces. The following expression has been proposed for the rate of thinning:

$$V = \frac{8}{3\mu}\sqrt[5]{\frac{4D^{12}\Delta P^8}{\alpha_1^{12}\sigma^3 r^4}} \tag{6}$$

Here, α_1 is the first root of the first-order Bessel function of the first kind and σ is the surface tension. Note that in Eq. (6), the rate of thinning is inversely proportional to $r^{4/5}$. This is in good agreement with some experimental observations.

III. SURFACE FORCES

At sufficiently small droplet separations, say below 100 nm, surface forces have to be considered. These forces affect the drainage rate as well as the equilibrium interactions, particularly if flocculation occurs. The most commonly encountered forces are briefly described in this section. For a general reference to surface force, see the book by Israelachvili (12).

A. Van der Waals Forces

Van der Waals forces originate from the motion of negatively charged electrons around the positively charged atomic nucleus. For condensed materials (liquids or solids), this electron motion gives rise to a fluctuating electromagnetic field that extends beyond the surface of the material. Thus, when, for example, two particles or emulsion droplets are close together, the fluctuating fields associated with them will interact with each other. The energy of interaction per unit area (W_{vdw}) between two equal spheres with radius R a distance D apart is given by:

$$W_{\text{vdw}} = -\frac{A}{6}\left[\frac{2R^2}{D^2+4RD} + \frac{2R^2}{D^2+4RD+R^2} + \ln\left(\frac{D^2+4RD}{D^2+4RD+R^2}\right)\right] \tag{7}$$

where A is the nonretarded Hamaker constant. When the particle radius is much larger than the separation of the particles, Eq. (7) is reduced to

$$W_{\text{vdw}} = -\frac{AR}{12D} \tag{8}$$

The Hamaker constant depends on the dielectric properties of the two interacting particles and the intervening medium. When these properties are known, one can calculate the Hamaker constant. An approximate equation for two identical particles (subscript 1) interacting across a medium (subscript 2) is:

$$A = \frac{3kT}{4}\left(\frac{\varepsilon_1 - \varepsilon_2}{\varepsilon_1 - \varepsilon_2}\right)^2 + \frac{3h\nu}{16\sqrt{2}}\left(\frac{(n_1^2 - n_2^2)^2}{(n_1^2 + n_2^2)^{3/2}}\right) \tag{9}$$

where k is the Boltzmann constant, T is the absolute temperature, ν is the main absorption frequency in the ultraviolet (UV) region (often about 3×10^{15} Hz), h is Planck's constant, ε is the static dielectric constant, and n is the refractive index in visible light.

From Eqs. (8) and (9), it is clear that the van der Waals interaction between two identical particles or emulsion droplets is always attractive. One may also note that the Hamaker constant for two oil droplets interacting across water is identical to the Hamaker constant for two water droplets interacting across oil.

B. Electrostatic Double-Layer Forces

Electrostatic double-layer forces are always present between charged particles or emulsion droplets in electrolyte solutions. Counterions to the emulsion droplet (ions with opposite charges to that of the drop) are attracted to the surfaces and co-ions are repelled. Hence, outside the charged emulsion droplet, in the so-called diffuse layer, the concentration of ions will be different than that in bulk solution, and the charge in the diffuse layer balances the surface charge.

An electrostatic double-layer interaction arises when two charged droplets are so close together that their diffuse layers overlap. The electrostatic double-layer interaction, W_{dl}, for two identical charged drops with a small electrostatic surface potential and a radius large compared to their separation is approximately given by

$$W_{\text{dl}} = 2\pi R\varepsilon\varepsilon_0\Psi_0^2 \exp(-\kappa D) \tag{10}$$

where ε_0 is the permittivity of vacuum, ε is the static dielectric constant of the medium, Ψ^0 is the surface potential, and κ^{-1} is the Debye screening length given by:

$$\kappa^{-1} = \sqrt{\frac{\varepsilon_0 \varepsilon k T}{1000 N_A e^2 \sum_i c_i z_i^2}} \tag{11}$$

where e is the charge of the proton, N_A is Avogadro's number, c_i is the concentration of ion i expressed as mol/dm^3, and z_i is the valeny of ion i.

The double-layer interaction is repulsive and it decays exponentially with surface separation with a decay length equal to the Debye length. Further, the Debye length and, consequently, the range of the double-layer force decreases with increasing salt concentration and the valency of the ions present. The famous Derjaguin Landau Verwey Overbeek (DLVO) theory for colloidal stability (13,14) takes into account double-layer forces and van der Waals forces.

C. Hydration and Steric-Protrusion Forces

Hydration and steric-protrusion forces are repulsive forces that have been found to be present at rather short separations between hydrophilic surfaces such as surfactant head groups. At least two molecular reasons for these forces have been identified. First, when two polar surfaces are brought close together, the polar groups will be partly dehydrated, which gives rise to a repulsive force (15). Second, as two surfaces are brought close together, the molecules at the interface will have a decreased mobility perpendicular to the surface, which decreases the entropy of the system, and this gives rise to a steric type of repulsion (16). Empirically, it has been found that the hydration/steric repulsion between surfactant and lipid head groups decays roughly exponentially with distance:

$$W_{\text{hyd}} = W_{\text{hyd}}^0 \exp\left(-\frac{D}{\lambda}\right) \tag{12}$$

where λ is the decay length of the force, typically 0.2–0.3 nm.

D. Polymer-Induced Forces

The presence of polymers on surfaces gives rise to additional forces that can be repulsive or attractive. Under conditions when the polymer is firmly anchored to the surface and the surface coverage is large, a steric

repulsion is expected. As the surfaces are brought together, the segment density between them increases, which results in an increased number of segment–segment contacts and a loss of conformational entropy of the polymer chains. The conformational entropy loss always results in a repulsive force contribution that dominates at small separations. The increased number of segment–segment contacts may give rise to an attractive or a repulsive force contribution. This is often discussed in terms of the chi-parameter (χ-parameter) or in terms of the solvent quality. Under sufficiently poor solvent conditions ($\chi > 1/2$), when the segment–segment interaction is sufficiently favourable compared to the segment–solvent interaction, the long-range interaction can be attractive. Otherwise, it is repulsive. The steric force can be calculated by using lattice mean field theory (17) or scaling theory (18). The actual force encountered is highly dependent on the adsorption density, the surface affinity, the polymer architecture, and the solvency condition. Hence, no simple equation can describe all situations. However, a high-density polymer layer, a ''brush'' layer, in a good solvent, provides good steric stabilization. The scaling approach provides us with a simple formula that often describes the measured interactions under such conditions rather well (19). It states that the pressure $P(D)$ between two flat polymer-coated surfaces is given by

$$P(D) \approx \frac{kT}{s^3}\left[\left(\frac{D^*}{D}\right)^{9/4} - \left(\frac{D}{D^*}\right)^{3/4}\right] \tag{13}$$

where Eq. (13) is valid provided that the separation, D, is less than D^* (where D^* is twice the length of the polymer tail), and s is the linear distance between the anchored chains on the surface. For the interactions between two spheres with a radius significantly larger than their separation, this relation is modified to

$$\frac{F(D)}{R} \approx -\pi \int_{D^*}^{D} P(D')\, dD' \tag{14}$$

The parameters needed to calculate the force are the length of the extended polymer chain and the separation between the polymer chains on the surface. The latter parameter can be estimated from the adsorbed amount, whereas the length of the polymer chains enters as a fitting parameter. The formula predicts a repulsion that increases monotonically with decreasing separation.

E. Coalescence and Hole Formation

When studying drainage and equilibrium interactions in single-foam films above the critical micellar concentration (cmc) of the surfactant, it is often found that the film thickness undergoes sudden changes (20,21). This phenomenon is known as stratification. Below the cmc, one sudden change from a water-rich common black film to a very thin Newton black film may occur. This transition does not occur uniformly over the whole film area but initially in some small regions. The thinner regions are often called black spots because they appear darker than the rest of the film when viewed in reflected light. Once formed, the size of a black spot grows as the liquid drains out from the foam lamellae. Bergeron and co-workers noted that the viscous resistance to the flow in the thin film is large and that this leads to an increase in the local film thickness next to the black spot (22,23). The suggested shape of the thin liquid layer, which is supported by experimental observations and theoretical calculations (22,23) is illustrated in Fig. 1. In many cases, no or unstable Newton black films are formed. In these cases, the films rupture due to formation of a hole that rapidly grows as a result of surface-tension forces. Emulsion coalescence occurs in a similar manner.

The mechanism of black spot formation and rupture has been extensively studied (24). It is generally recognized that the liquid film is unstable in regions of the disjointing pressure (Π) isotherm (force curve) where the derivative with respect to film thickness (D) is larger than zero (i.e., $d\Pi/dD > 0$). Hence, close to a maximum in the disjoining pressure isotherm (see Fig. 2), a small disturbance causing a change in film thickness and/or capillary pressure may spontaneously grow and lead to significant change in film thickness (e.g., Newton black film formation or rupture).

The stability of foams and emulsions depends critically on whether formation of a stable Newton black film or a hole leading to coalescence is favored. Kabalnov and Wennerström (4) addressed this question by

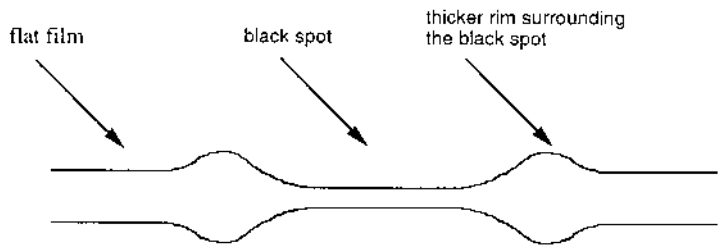

Figure 1 Illustration of shape of the thin liquid film around the position of a newly formed black spot.

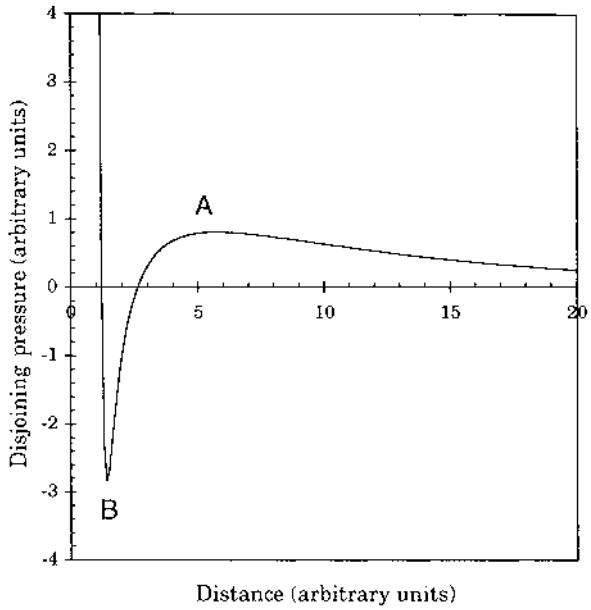

Figure 2 Typical disjoining pressure isotherm showing one maximum (A) and one minimum (B); the film is unstable between points A and B.

developing a temperature-induced hole nucleation model. They point out that the coalescene energy barrier is strongly affected by the spontaneous monolayer curvature. The authors consider a flat emulsion film, covered by a saturated surfactant monolayer, in thermodynamic equilibrium with a micellar bulk solution. The emulsion breaks if an induced hole grows along the film having a thickness $h = 2b$ (Fig. 3). The change in free energy occurring when a hole is formed is given as the difference in the interfacial tension integrals over the interface for a film with a hole compared to that for a planar film:

$$W = \int_{\text{(film with hole)}} \sigma(x, y, z)\, dA - \int_{\text{(flat film)}} \sigma(x, y, z)\, dA \tag{15}$$

The diving force for the formation of a hole is the reduction in free energy owing to a decrease in surface area of the planar part of the film, whereas it is counteracted by the increased free energy due to the surface area created around the hole. In general, the change in free energy goes through a maximum as the hole radius increases. One new feature of the Kabalnov–Wennerström model is that the surface tension at the hole edge is

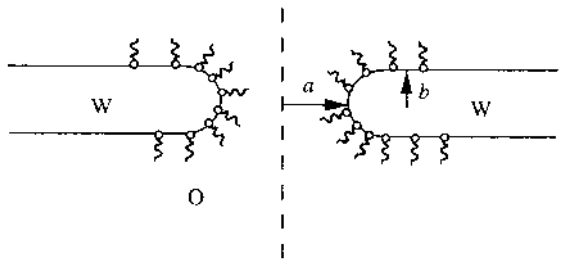

Figure 3 Geometry of the thin film just after a hole has been created. (Redrawn from Ref. 4, with permission.)

considered to be different than that at the planar film surface. The reason for this is that the curvature of the interface is different, leading to a difference in surfactant monolayer bending energy. This can be expressed as (4)

$$\sigma^{\text{curved}} = \sigma^{\text{planar}} + 2\kappa(H - H_0)^2 - 2\kappa H_0^2 \tag{16}$$

Here, H and H_0 are the mean and the spontaneous curvatures and κ is the bending modulus.

Clearly, the surface tension has a minimum when the spontaneous curvature of the surfactant film equals the mean curvature of the interface. The mean curvature for a flat interface is zero, larger than zero for an interface curving toward the oil (oil-in-water emulsions), and smaller than zero for a water-in-oil emulsion. Hence, a large positive spontaneous monolayer curvature, as for a strongly hydrophilic surfactant, favors oil-in-water emulsions and vice versa. The Kabalnov–Wennerström model also allows the thickness of the film to vary in order to minimize the free energy of hole formation (i.e., the mean curvature of the film close to the hole can approach the spontaneous monolayer curvature). The Kabalnov–Wennerström model has to be solved numerically in order to calculate the coalescence activation energy. However, a ''big hole approach'' where $a \gg b$ (see Fig. 3) gives surprisingly good results. In this model, the energy for creating a hole with radius a is given as

$$W = 2\pi a\gamma - 2\pi a^2\sigma \tag{17}$$

where $2\pi a$ is the circumference of the hole, γ is the line tension, πa^2 is the area of the hole at each interface, and σ is the surface tension. The second term is the free energy gain by reducing the flat area of the film, and the first term is the energy penalty of creating the inside of the hole. The value of the

line tension can be calculated when the spontaneous monolayer curvature and the monolayer bending modulus is known (4). The activation energy of coalescence (W^*) is obtained by finding the point where $dw/da = 0$, which gives the final expression:

$$W^* = \frac{\pi\gamma^2}{2\sigma} \tag{18}$$

The particular feature with ethylene oxide-based surfactants is that their interaction with water is less favourable at higher temperatures. This leads to a decrease in the spontaneous monolayer curvature with temperature, explaining the transition from oil-in-water emulsions below the PIT to water-in-oil emulsion above the PIT. In the vicinity of the PIT, the energy barrier against coalescence (W^*) varies very strongly with temperature. For the system *n*-octane–$C_{12}E_5$–water, the following approximate relation was obtained in terms of $\Delta T = T - T_d$, where T_d is the PIT (4):

$$\frac{W^*}{kT} = 0.43 + 30.9|\Delta T| \tag{19}$$

The predicted very steep increase in the coalescence barrier away from the PIT is qualitatively in good agreement with the experimentally observed macroemulsion behavior (25).

IV. SURFACE FORCE TECHNIQUES

There are several methods available for measuring forces between two solid surfaces, two particles, or liquid interfaces (26). In this section, we briefly mention some of the features of the techniques that have been used in order to produce the results described in the later part of this chapter. The forces acting between two solid surfaces were measured either with the interferometric surface force apparatus (SFA) or with the MASIF (measurements and analysis of surface and interfacial forces). Interactions between fluid interfaces were determined using various versions of the thin-film pressure balance (TFB).

A. Interferometric Surface Force Apparatus

The forces acting between two molecularly smooth surfaces, normally mica or modified mica, can be measured as a function of their *absolute* separation with the interferometric SFA (Fig. 4) (27). This provides a convenient way to measure not only long-range forces but also the thickness of adsorbed

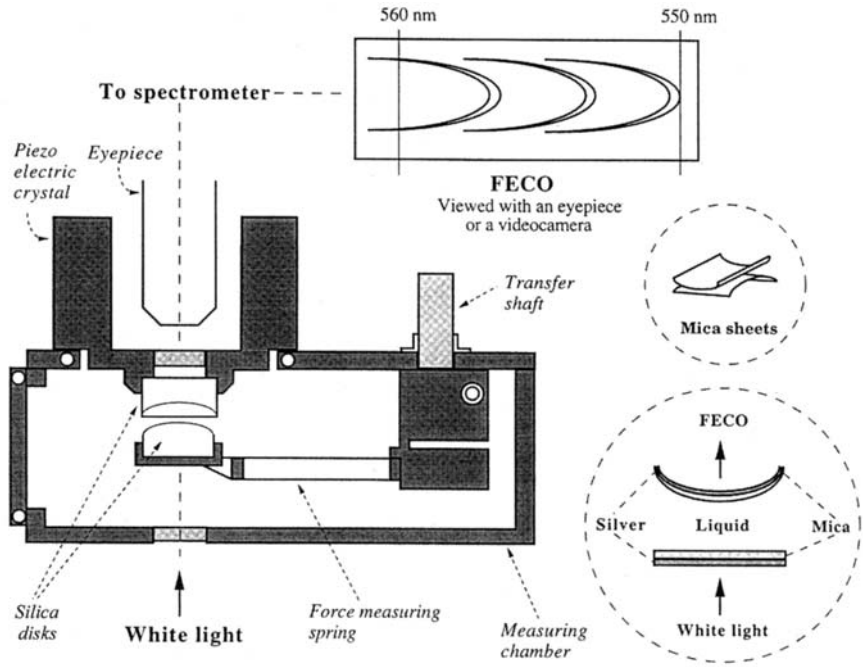

Figure 4 Schematic of a surface force apparatus (SFA). The measuring chamber is made from stainless steel. One of the surfaces is mounted on a piezoelectric tube that is used to change the surface separation; the other surface is mounted on the force measuring spring. (From Ref. 26, with permission.)

layers. The absolute separation is determined interferometrically to within 0.1–0.2 nm by using fringes of equal chromatic order. The surfaces are glued on optically polished silica disks and mounted in the SFA in a crossed cylinder configuration. The surface separation is controlled either by adjusting the voltage applied to a piezoelectric crystal rigidly attached to one of the surfaces or by a synchronous motor linked by a cantilever spring to the other surface. The deflection of the force-measuring spring is also determined interferometrically, and the force is calculated from Hooke's law. For further details, see Ref. 27.

When an attractive force component is present, the gradient of the force with respect to the surface separation, $\partial F/\partial D$, may at some distance become larger than the spring constant, k. The mechanical system then enters an unstable region causing the surfaces to jump to the next stable point (compare instabilities in free liquid films that occur when $d\Pi/dD > 0$). The adhesion force, $F(0)$, normalized by the local mean radius of curvature,

R, is determined by separating the surfaces from adhesive contact. The force is calculated from

$$\frac{F(0)}{R} = \frac{kD_j + F(D_j)}{R} \tag{20}$$

where $F(D_j)$ is the force at the distance (D_j) to which the surfaces jumped on separation, and R is the mean radius of the surfaces.

B. The Bimorph Surface Force Apparatus

The force as a function of the surface separation between glass substrate surfaces was measured with a MASIF instrument (28). This apparatus is based on a bimorph force sensor to which one of the surfaces is mounted (Fig. 5). The other surface is mounted on a piezoelectric tube. The bimorph (enclosed in a Teflon sheath) is mounted inside a small measuring chamber, which is clamped to a translation stage that serves to control the coarse position of the piezoelectric tube and the upper surface.

The voltage across the piezoelectric tube is varied continuously and the surfaces are first pushed together and then separated. The bimorph will deflect when a force is experienced and this generates a charge in proportion to the deflection. From the deflection and the spring constant, the force follows simply from Hooke's law. The motion of the piezo is measured during each force run with a linear displacement sensor. The signal together with the signal from the bimorph charge amplifier, the voltage applied to the piezoelectric tube, and the time are recorded by a computer. The speed of approach, the number of data points, and other experimental variables can easily be controlled with the computer software.

When the surfaces are in contact, the motion of the piezoelectric tube is transmitted directly to the force sensor. This results in a linear increase of the force sensor signal with the expansion of the piezoelectric tube. The sensitivity of the force sensor can be calibrated from this straight line, and this measuring procedure allows the determination of forces as a function of separation from a hard wall contact with a high precision (within 1–2 Å in distance resolution). Note, however, that the assumption of a "hard wall" contact is not always correct (29).

The MASIF instrument does not use interferometry to determine surface separations, which leads to the drawback that the layer thickness cannot be determined, but to the advantage that the instrument can be used with any type of hard, smooth surfaces. In most cases, spherical glass surfaces are used. They are prepared by melting a 2-mm-diameter glass rod until a molten droplet with a radius of 2 mm is formed.

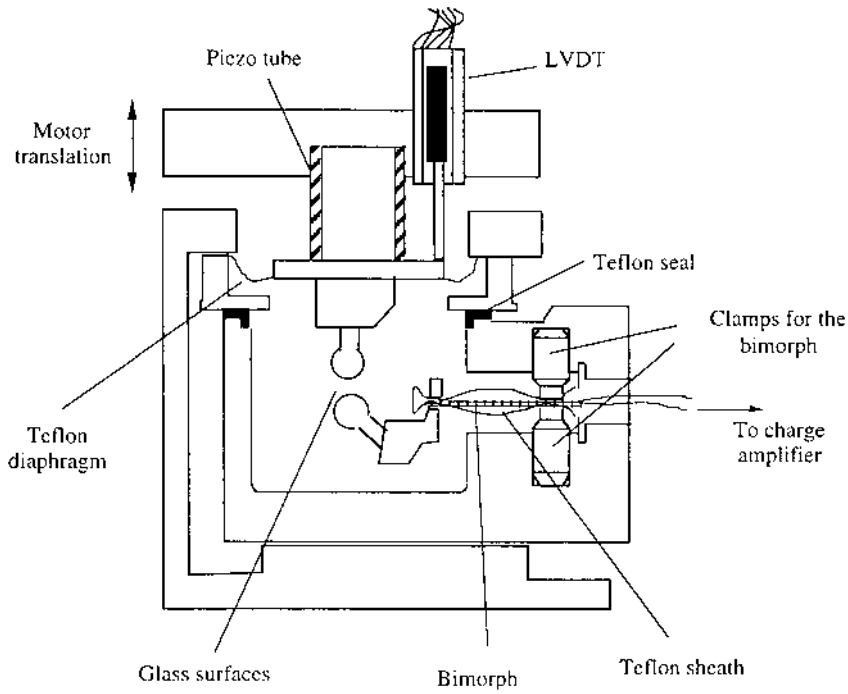

Figure 5 Schematic of the MASIF instrument. The upper surface is mounted on a piezoceramic actuator that is used for changing the surface separation; the hysteresis of the piezoexpansion/contraction cycle can be accounted for by using a linear variable displacement transducer (LVDT). The lower surface is mounted on a bimorph force sensor. (From Ref. 26, with permission.)

C. Derjaguin Approximation

The force measured between crossed cylinders (F_c), as in the SFA, and between spheres (F_s), as in the MASIF, a distance D apart is normalized by the local geometric mean radius (R). This quantity is related to the free energy of interaction per unit area between flat surfaces (W) according to the Derjaguin approximation (30):

$$\frac{F_c}{2\pi R} = \frac{F_s}{\pi R} = W \tag{21}$$

This approximation is valid when the radius (about 2 cm in the SFA and 2 mm in the MASIF) is much larger than the surface separation (typically 10^{-5} cm or less), a requirement fulfilled in these experiments. With the SFA,

the local radius is determined from the shape of the standing-wave pattern, whereas in the MASIF, we have used the assumption that the local radius is equal to the macroscopic radius, determined using a micrometer. The radius used in Eq. (21) is that of the undeformed surfaces. However, under the action of strongly repulsive or attractive forces, the surfaces will deform and flatten (31,32). This changes the local radius and invalidates Eq. (21) because R becomes a function of D.

D. Thin-Film Pressure Balance

Accurate information about the rate of thinning, the critical thickness of rupture, and the forces acting between two air–water interfaces, between two oil–water interfaces, and between one air–water and one oil–water interface can be gained by using thin-film pressure balance techniques. The thickness of the separating water film is determined by measuring the intensity of reflected white light from a small flat portion of the film (33). Due to interference of the light reflected from the upper and lower film surfaces, characteristic interference colors are observed during the thinning. These colors correspond to a shift in the wavelengths undergoing constructive and destructive interference. When such a process is recorded (normally as intensity of a given light wavelength versus time), a sequence of intensity minima and maxima appears. The equivalent water film thickness can be calculated from the following equation (33):

$$h_{\text{eq}} = \left(\frac{\lambda}{2\pi n_1}\right) \arcsin\left(\sqrt{\frac{\Delta}{1 + [4R(1-\Delta)/(1-R)^2]}}\right)$$

$$R = \left(\frac{n_1 - n_2}{n_1 + n_2}\right)^2 \tag{22}$$

$$\Delta = \left(\frac{I - I_{\min}}{I_{\max} - I_{\min}}\right)$$

where λ is the wavelength and n_1 and n_2 are the bulk refractive indices of the continuous and the disperse phases respectively (in the case of foam films $n_2 = 1$); $I_{\max}$ and $I_{\min}$ are the intensity values of the interference maximum and minimum, and I is the instantaneous value of the light intensity. The above equation gives the equivalent film thickness, h_{eq} (i.e., the film thickness plus the thickness of the adsorbed layers calculated by assuming a constant value of the refractive index equal to n_1). A better approximation to the true film thickness can be obtained by correcting for the difference in

refractive index between the bulk film and the adsorbed layer. The corrected film thickness is (23)

$$h = h_{eq} - 2h_{hc}\left(\frac{n_{hc}^2 - n_1^2}{n_1^2 - n_2^2}\right) - 2h_{pg}\left(\frac{n_{pg}^2 - n_1^2}{n_1^2 - n_2^2}\right) \tag{23}$$

In Eq. (23), h_{hc} and h_{hg} are the thickness of the region occupied by the surfactant hydrocarbon chain and polar group, respectively. Similarly, n_{hc} and n_{pg} are the corresponding refractive indices. The thickness values needed in order to use Eq. (23) can be estimated from the volume of the two parts of the molecule together with values of the area per molecule at the interface obtained from adsorption data (e.g., the surface-tension isotherm). Finally, the thickness of the core layer (water in the case of foam films) can be calculated as

$$h_{core} = h - 2(h_{hc} + h_{pg}) \tag{24}$$

The apparatus used for studying thin liquid films is schematically depicted in Fig. 6. This device, commonly known as a thin-film pressure balance, allows drainage patterns of single foam, emulsion, or wetting films

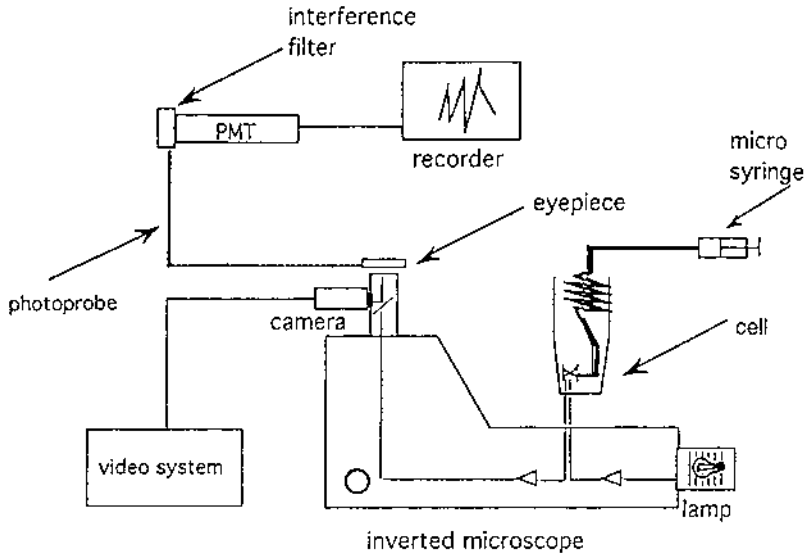

Figure 6 Schematic of the main components of a typical thin-film pressure balance.

to be recorded. The film is formed in a specially constructed cell that is placed on the stage of an inverted microscope. The reflected light from the film is split into two parts: one directed to a charge-coupled device (CCD) camera and another to a fiber-optic probe tip located in the microscope eyepiece. The radius of the tip is only about 20 μm, which allows light from a small portion of the film to be registered. The light signal is then passed through a monochromatic filter and, finally, directed on to a high-sensitivity photomultiplier. The output of the photomultiplier is connected to a chart recorder and the data are collected in the form of intensity (as a photocurrent) versus time. This graph is called an interferogram.

An essential part of the thin-film balance is the cell holding the thin film. The cell can be constructed in several ways depending on the type of measurement to be done and the systems under investigation. For, emulsion films, the type of cell proposed by Scheludko (33) is often used. The cell is illustrated in Fig. 7. The film is formed between the tips of the menisci of a biconcave drop held in a horizontal tube with radius 1.5–2 mm. The tube and the spiral capillary are filled with the aqueous phase and immersed in a cuvette (the lower part of the cell) containing the oil phase. A small suction pressure applied through the capillary controls the film radius. Recently, a cell that is similar to that of Scheludko, but miniaturized about 10-fold was used by Velev et al. (34). This allowed film sizes and capillary pressures found in real emulsion systems to be studied. Bergeron and Radke (35)

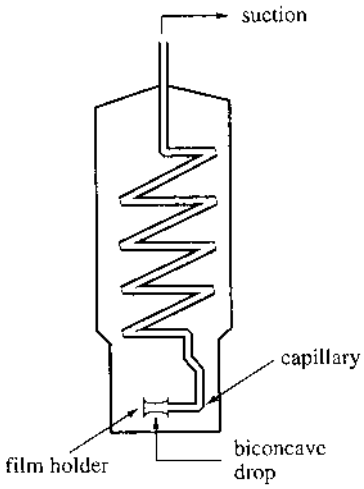

Figure 7 Illustration of the Scheludko cell used for investigation of single, horizontal foam and emulsion films.

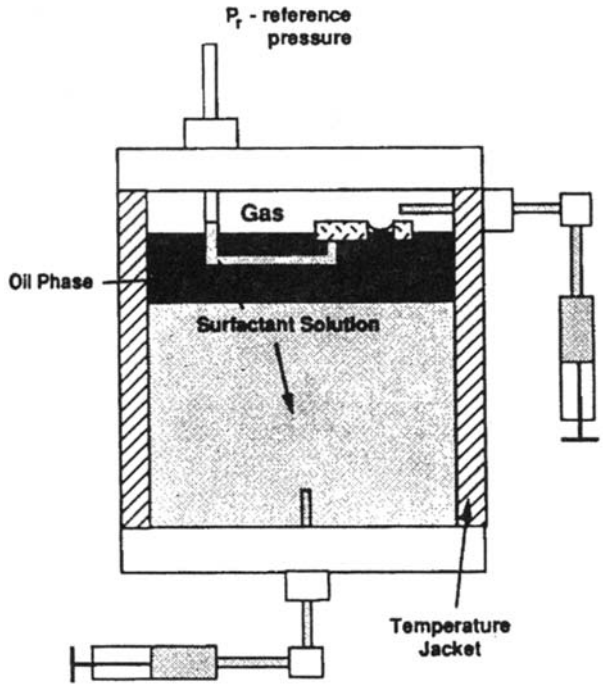

Figure 8 Modified porous-plate cell for investigation of pseudoemulsion films. (Ref. 35, with permission.)

used a cell with a porous frit holder as suggested by Mysels and Jones (36) for measuring equilibrium forces across foam and pseudoemulsion films. Their construction is shown in Fig. 8. The main advantage of this so-called porous-plate technique is that one can vary the pressure in the film by simply altering the gas pressure in the cell, and thus the stable part of the equilibrium disjoining pressure isotherm (where $d\Pi/dD < 0$) can be obtained.

V. RESULTS AND DISCUSSION

A. Ionic Surfactants on Hydrophobic Surfaces

Many oil-in-water emulsions are stabilized by an adsorbed layer of surfactants. One example is asphalt oil-in-water emulsions that often are stabilized by cationic surfactants (37). The surfactants fulfill two purposes. First, they generate long-range repulsive forces which prevent the emulsion droplets

from coming close to each other. Second, the surfactant layer acts as a barrier against coalescence if the emulsion droplets by chance come close to each other despite the long-range repulsive forces. The coalescence is hindered by a high spontaneous monolayer curvature, monolayer cohesive energy, surface elasticity, and surface viscosity, which increase the activation energy for hole formation and slow down the depletion of surfactants from the contact region. The importance of the cohesive energy for foam films stabilized by a homologous series of cationic surfactants was particularly clearly demonstrated by Bergeron (38). We note that an increased cohesive energy in the monolayer increases the bending modulus and thus the free energy cost for the surfactant film to have a curvature different than the spontaneous curvature.

Surface force measurements using a hydrophobic solid surface as a model for a fluid hydrocarbon–water interface provide a good picture of the long-range forces acting between emulsion droplets. However, the coalescence behavior of emulsions will not be accurately described from such measurements. One reason is that the fluid interface is much more prone to deformation than the solid surface (facilitating hole formation), and the surfactant chains can readily penetrate into the fluid oil phase but not into the solid hydrocarbon surface. Further, the mobility of the surfactants on a solid hydrophobic surface will be different than the mobility at a fluid interface.

The forces acting between two hydrophobic surfaces across dodecylammonium chloride surfactant solutions are illustrated in Fig. 9 (39). The long-range repulsion is due to the presence of an electrostatic double-layer force. This force is generated by the cationic surfactants that adsorb to the hydrophobic surface thereby generating a surface charge density. The range of the double-layer force decreases with increasing surfactant concentration, which is simply a result of the increased ionic strength of the aqueous media. On the other hand, the magnitude of the double-layer force at short separations increases with increasing surfactant concentrations. This is a consequence of the increased adsorption of the ionic surfactant that results in an increase in surface charge density and surface potential. The surfactant concentration will influence the long-range interactions between oil-in-water emulsions in the same way as observed for the model solid hydrophobic surfaces; that is, the range of the double-layer force will decrease and the magnitude of the force at short separations will increase. However, the adsorbed amount at a given surfactant concentration may not be the same on the emulsion surface as on the solid hydrophobic surface.

At low surfactant concntrations, it is observed that an attraction dominates at short separations. The attraction becomes important at separations below about 12 nm when the surfactant concentration is 0.01 mM, and

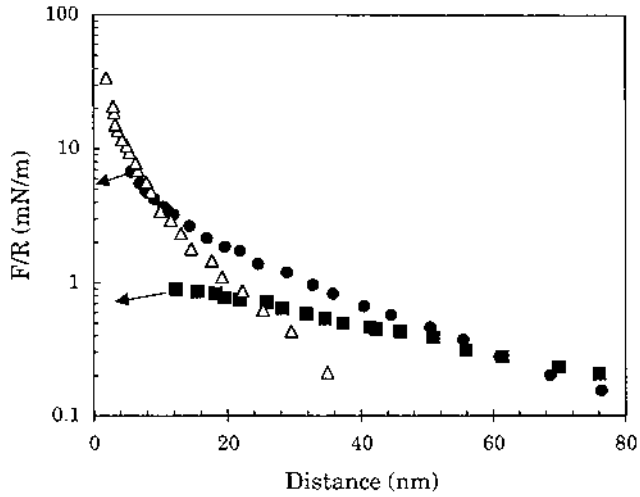

Figure 9 Force normalized by radius measured between two hydrophobized mica surfaces in crossed cylinder geometry across aqueous solutions of dodecylammonium chloride; the surfactant concentration was 0.01 mM (■), 0.1 mM (●), and 1 mM (△), respectively. The arrows indicate inward jumps occurring when the force barrier has been overcome. (Redrawn from Ref. 39, with permission.)

below about 6 nm when the concentration is increased to 0.1 mM. Once the force barrier has been overcome, the surfaces are pulled into direct contact between the hydrophobic surfaces at $D = 0$, demonstrating that the surfactants leave the gap between the surfaces. The solid surfaces have been flocculated. However, at higher surfactant concentrations (1 mM) the surfactants remain on the surfaces even when the separation between the surfaces is small. The force is now purely repulsive and the surfaces are prevented from flocculating. Emulsion droplets interacting in the same way would coalesce at low surfactant concentrations once they have come close enough to overcome the repulsive barrier, but remain stable at higher surfactant concentrations. Note, however, that the surfactant concentration needed to prevent coalescence of emulsion droplets cannot be accurately determined from surface force measurements using solid surfaces.

For application purposes, it is often found that asphalt emulsions stabilized by cationic surfactants function better than such emulsions stabilized by anionic surfactants. One main reason is that the interaction between the emulsion droplet and the road material differs depending on the emulsifier used (37). When the asphalt emulsion is spread on the road surface, it should rapidly break and form a homogeneous layer. The stones on the road surface are often negatively charged and there will be an electrostatic

attraction between cationic emulsion droplets and the stones. This attraction facilitates the attachment and spreading of the emulsion. On the other hand, when the emulsion droplet is negatively charged, there will be an electrostatic repulsion between the stones and the emulsion droplets.

B. Nonionic Surfactants on Hydrophobic Surfaces

Nonionic ethylene oxide-based surfactants are commonly used as emulsifiers. Because these surfactants are uncharged, they are not able to generate stabilizing long-range electrostatic forces. Instead, they generate short-range hydration/protrusion forces that prevent the emulsion droplets from coming into direct contact with each other. The short-range forces acting between hydrophobic solid surfaces coated with such surfactants as a function of temperature are illustrated in Fig. 10 (40). The zero distance in the diagram is defined as the position of the hard wall (at a value of $F/R \approx 100\,\text{mN/m}$).

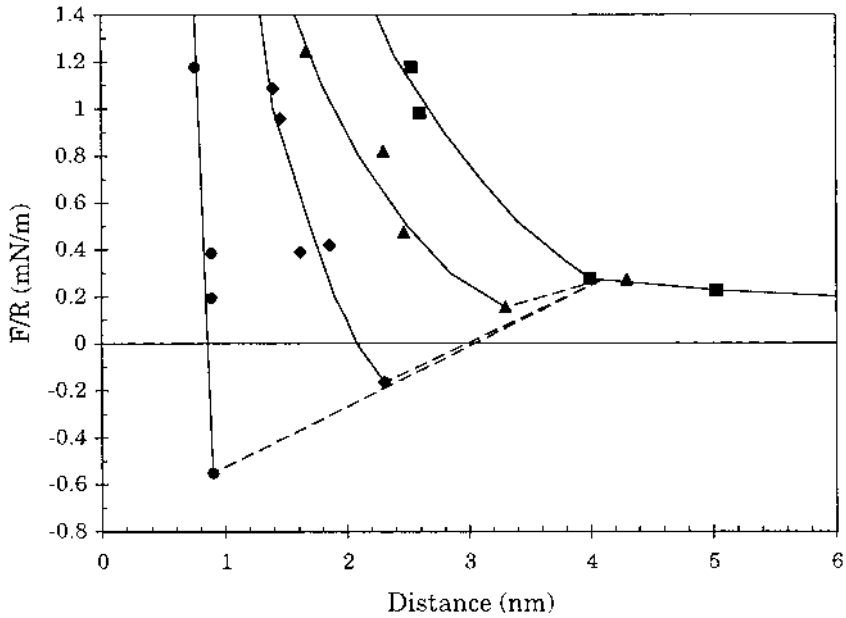

Figure 10 Force normalized by radius measured between hydrophobized mica surfaces in crossed cylinder geometry across a 6×10^{-5} M aqueous solution of penta(oxyethylene) dodecyl ether. The temperatures were 15°C (■), 20°C (▲), 30°C (◆), and 37°C (●). The lines are guides for the eye. (Redrawn from Ref. 40, with permission.)

The force present at distances above 4 nm is a weak double-layer force. It originates from remaining charges on the hydrophobic substrate surface. The force observed at smaller separations has a pronounced temperature dependence. It becomes less repulsive with increasing temperature. At the same time, the adsorbed layer thickness increases, demonstrating that the repulsion between the adsorbed molecules within one layer is also reduced at higher temperatures, facilitating an increased adsorption. The increase in layer thickness is not seen in Fig. 10 due to our definition of zero separation.

A decreasing interlayer and intralayer repulsion with increasing temperature is common for all surfactants and polymers containing oligo(ethylene oxide) groups. This shows that the interaction between ethylene oxide groups and water becomes less favorable at higher temperatures (i.e., the ethylene oxide chain becomes more hydrophobic). There are several theoretical attempts to explain this phenomenon, but it is outside the scope of this chapter to discuss them and the reader is referred to the original literature (41–48). The temperature dependence of the interaction between oligo(ethylene oxide) chains and water has several important consequences. The micellar size increases with temperature (49), and the micellar solution has a lower consolute temperature (i.e., a phase separation occurs on heating) (50). The cloud points for a range of micellar alkyl ethoxylate solutions are

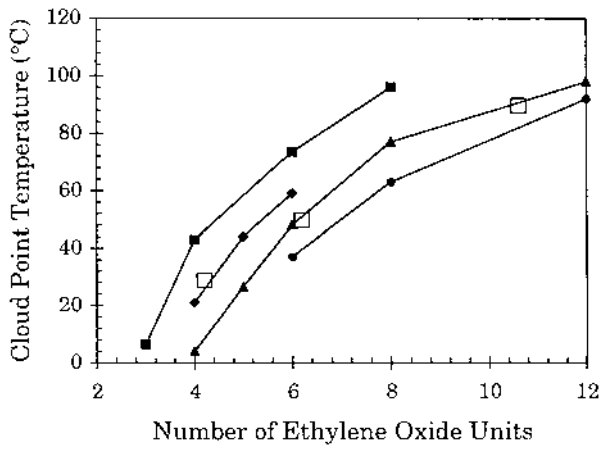

Figure 11 Cloud point temperature of micellar solutions as a function of the ethylene oxide chain length: the hydrophobic part is an alkyl chain with 8 (■), 10 (◆), 12 (▲), or 16 (●) carbon atoms. (Data from Ref. 51.) The symbols (□) represent the phase-inversion temperature for a 1 : 1 cyclohexane–water emulsion containing 5% commercial ethylene oxide-based emulsifiers having dodecylalkyl chains as a hydrophobic group. (Data from Ref. 54.)

provided in Fig. 11 (51). The cloud point increases with the number of ethylene oxide units. The reason is that a longer ethylene oxide chain gives rise to a longer-range intermicellar repulsion and a larger optimal area per head group (favoring smaller micelles). On the other hand, the cloud point decreases with the length of the hydrocarbon chain. By considering the geometry of the surfactant as described by the packing parameter (52), one realizes that the micellar size is expected to increase with the hydrocarbon chain length. It is also found that surfaces coated with (ethylene oxide containing) polymers often have good protein-repellent properties at low temperatures, whereas proteins adsorb more readily to such surfaces at higher temperatures (53).

For emulsions the most important aspect may be that the optimal area per head group in an adsorbed layer decreases with increasing temperature, which reduces the spontaneous monolayer curvature (4). This is the reason why emulsions stabilized by ethylene oxide-based surfactants may change from oil-in-water to water-in-oil when the temperature is increased. The temperature when this occurs is known as the phase-inversion temperature (PIT). The PIT depends on the length of the hydrocarbon chain and the ethylene oxide chain in a manner similar to the cloud point (54) (see Fig. 11). However, the PIT also depends on the type of oil used (55), which is partly due to differences in solubility of the ethylene oxide surfactants in the different oils and to differences in oil penetration in the surfactant layer. We also note that if the emulsifier concentration is high enough, a liquid-crystalline phase may accumulate at the oil–water interface. In such cases, emulsions which are very stable toward coalescence may be formed (56). This is a result of the decreased probability of hole formation (4). In this case, the type of oil used has a dramatic effect on the emulsion stability, which can be understood by considering the three-component phase diagram.

C. Nonionic Polymers on Hydrophobic Surfaces

Earlier, we discussed how the length of the oligo(ethylene oxide) chain influences the properties of emulsions stabilized by alkyl ethoxylates. When the ethylene oxide chain becomes sufficiently long, one normally refers to the substance as a diblock copolymer rather than as a surfactant. Of course, there is no clear distinction, but the properties vary in a continuous fashion with increasing ethylene oxide chain length. It is of interest to follow how the forces acting between two surfaces carrying adsorbed diblock copolymers vary with the length of the adsorbing (anchor) block and the nonadsorbing (buoy) block. A nice experimental work addressing this question is that of Belder et al (57). Fleer et al. give a thorough theoretical treatment in their book (17), where it was suggested that the most

efficient steric stabilization is obtained when the anchor block has a size that is 10–20% of that of the buoy block. The reason for this optimum is that when the anchor block is too small, the driving force for adsorption is weak and the adsorbed amount will be low. On the other hand, when the anchor block is too large, the area per adsorbed molecule will be large. As a consequence, the buoy block layer will be dilute and it will not extend very far out into the solution, leading to a not very pronounced steric force.

The forces acting between solid hydrophobic surfaces coated with different ethylene oxide-based diblock polymers are illustrated in Fig. 12. The forces acting between surfaces coated with penta(oxyethylene) dodecyl ether, $C_{12}E_5$, becomes significantly repulsive at distances below about 2 nm, calculated from the hard wall contact at $D = 0$. Note that the surfactant layer remains between the surfaces, and the range of the force given is thus relative to the position of direct contact between the compressed adsorbed surfactant layers. The forces between hydrophobic surfaces coated with a diblock copolymer containing 8 butylene oxide units and 41 ethylene oxide units, B_8E_{41}, are significantly longer ranged. The interaction at distances above 4 nm from the "hard wall" is dominated by a weak electrostatic double-layer force originating from remaining charges on the silanated glass surface. However, at shorter distances, a steric force predominates.

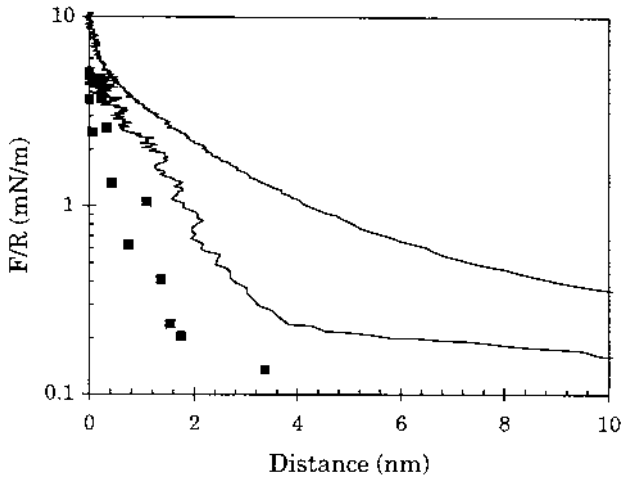

Figure 12 Force normalized by radius between hydrophobized mica or glass surfaces coated by penta(oxyethylene) dodecyl ether at 20°C (■), and copolymers of butylene oxide (B) and ethylene oxide (E) with compositions B_8E_{41} (lower line) and $B_{15}E_{200}$ (upper line). All data have been recalculated to spherical geometry.

Hence, the molecules with the longer ethylene oxide chains give rise to a longer-range force. Note that this is true even when the range is calculated from the position of the hard wall (i.e., without considering the difference in compressed layer thickness). A much longer-range force is observed in the case of $B_{15}E_{200}$, where the steric force extends to more than 10 nm away from the hard wall contact.

From the above, it is clear that rather large diblock copolymers are efficient in generating long-range repulsive steric forces, which is beneficial for increasing the stability of dispersed particles and emulsion droplets. An even higher stability may be obtained if a mixture of diblock copolymers and charged surfactants are used, thus providing both steric and electrostatic stabilization.

D. Polyelectrolytes on Surfaces

Both steric and electrostatic stabilization was utilized by Fäldt et al. (58) when making soybean oil emulsions. They first made the emulsion using a mixture of phosphatidylcholine and glycoholic acid (bile salt) with a pK_a of 4.4. The emulsion droplets obtained a net negative surface charge due to dissociation of the glycoholic acid. To improve the stability of the emulsion a weak cationic polyelectrolyte, chitosan, with a pK_a of 6.3–7 was added. The polyelectrolyte adsorbs to the negatively charged emulsion droplet surface, which becomes positively charged at low pH. It was found that the emulsion was stable at high and low pH but not at pH values around 7, where irreversible aggregation was observed. This clearly shows that the forces acting between the emulsion droplets change with pH. To shed light on this behavior, the forces acting between negatively charged solid surfaces coated by chitosan were measured as a function of pH (Fig. 13).

A repulsive double-layer force dominated the long-range interaction at pH values below 5. However, at distances below about 5 nm, the measured repulsive force is stronger than expected from DLVO theory due to the predominance of a steric force contribution. The layer thickness obtained under a high compressive force was 1 nm per surface. Hence, it is clear that positively charged chitosan adsorbs in a very flat conformation on strongly oppositely charged surfaces such as mica with only short loops and tails. When the pH is increased to 6.2, the mica–chitosan system becomes uncharged, because the charge density of the chitosan molecules has decreased. The decrease in charge density of the chitosan also results in a decrease in segment–segment repulsion and, therefore, an even more compact adsorbed layer. At this pH value, there is an attraction between the layers at a surface separation of about 2 nm. The steric repulsion is, in this

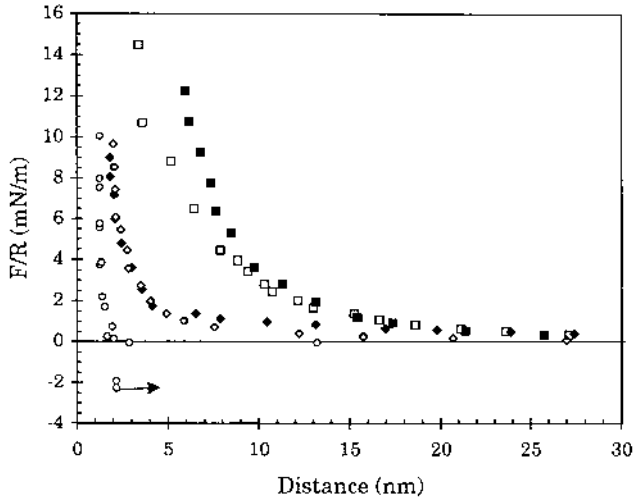

Figure 13 Force normalized by radius between negatively charged mica surfaces in crossed cylinder geometry precoated with a layer of chitosan, a cationic polyelectrolyte. The forces were recorded at pH 3.8 (◆), 4.9 (◇), 6.2 (○), 7.6 (□), and 9.1 (■); the arrow indicates an outward jump. (From Ref. 58, with permission.)

case, very short range (< 2 nm) and steep. A further increase in pH to 9.1 results in a recharging due to the fact that the charges on the polyelectrolyte no longer can compensate for all of the mica surface charges. Further, as the charge density of the polyelectrolyte is reduced, the range of the steric force increases again due to the lower affinity of the polyelectrolytes for the surface. Clearly, the mica–chitosan system is positively charged at low pH (i.e., the charges on the polyelectrolyte overcompensate for the charges on the mica surface), uncharged at pH 6.2, and negatively charged at high pH due to an undercompensation of the mica surface charge by the polyelectrolyte charges.

The flocculation behavior of the soybean emulsion can now be better understood. A stable emulsion is formed by a low pH owing to the electrostatic repulsion generated by the excess charges from the adsorbed chitosan. An intermediate pH values, the soybean emulsion is uncharged and the adsorbed chitosan layer is very flat. Hence, no long-range electrostatic force or long-range steric force is present that can stabilize the emulsion. At a high pH, the charges due to ionization of the glycoholic acid are no longer compensated for by the high pH at nearly uncharged chitosan. Thus, stablizing electrostatic forces are once again present. Further, the range of the stabilizing steric force is most likely also increased.

E. Proteins on Hydrophobic Surfaces

Amphiphilic proteins have properties similar to those of block copolymers and surfactants in the sense that they have clearly separated hydrophilic and hydrophobic domains that allow the formation of monodisperse aggregates or micelles in solution. For β-casein, the association process starts at a protein concentration of around 0.5 mg/mL at room temperature (59). Amphiphilic proteins adsorb strongly to nonpolar surfaces in contact with aqueous solutions, and they may generate stabilizing steric and electrostatic forces. In fact, caseins isolated from milk are widely used in different technical products ranging from food to paint and glue. One reason for this is that the caseins have excellent properties as emulsifiers and foaming agents, and emulsions stabilized by proteins constitute the most important class of food colloids. The caseins protect the oil droplets from coalescing and also provide long-term stability during storage and subsequent processing (60). β-Casein is more hydrophobic compared to the other caseins and the charged domain is clearly separated from the hydrophobic part, which makes the β-casein molecule, as whole, distinctly amphiphilic (61). At pH 7, the isolated β-casein molecule carries a net charge of about −12 (61).

Nylander and co-workers investigated the interactions between adsorbed layers of β-casein in order to clarify the mechanism responsible for the ability of β-casein to act as a protective colloid (62,63). The force as a function of surface separation between hydrophobic surfaces across a solution containing 0.1 mg/mL β-casein and 1 mM NaCl (pH = 7) is illustrated in Fig. 14. At separations down to about 25 nm, an electrostatic double-layer force dominates the interacation. The hydrophobic substrate surface was uncharged, so the charges responsible for this force had to come from the adsorbed protein. When the surfaces are compressed closer together, the repulsive force is overcome by an attraction at a separation of about 25 nm, and the protein-coated surfaces are sliding into contact about 8 nm out from the hydrophobized mica surface (Fig. 14, inset). This observation, as well as the adhesive force found on separation, was interpreted as being due to bridging of the hydrophilic tails that extend out into solution. Further compression does not significantly change the surfaces separation. The results indicate that the adsorbed β-casein layer consists of an inner compact part and a dilute outer region.

This conclusion compares favorably to what is known from studies of the adsorption of β-casein on to air–liquid, liquid–liquid, and solid–liquid interfaces using a range of other techniques. It has generally been found that the adsorbed amount of β-casein on hydrophobic surfaces is between 2 and 3 mg/m^2 over a wide range of bulk concentrations. This is the case for planar

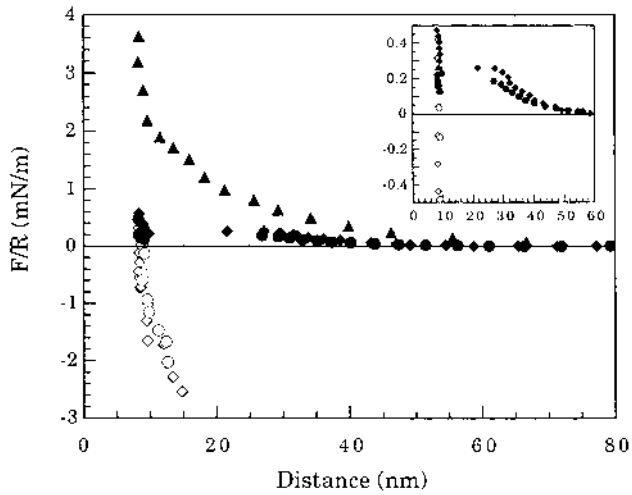

Figure 14 Normalized force measured between hydrophobized mica surfaces in crossed cylinder geometry coated with β-casein in a solution containing 0.1 mg β-casein/mL (pH = 7; 1 mM NaCl) (◆, ◇) and after dilution with 1 mM NaCl (●, ○). Filled and unfilled symbols represent the force measured on compression and decompression, respectively; ▲ represents, the force measured between hydrophobized mica surfaces across a 0.1-mM NaCl solution at pH 5.6 containing 0.2 mg proteoheparan sulfate/mL. The inset shows the measured forces between adsorbed layers of β-casein before and after dilution with 1 mM NaCl on an expanded scale. (From Ref. 26, with permission.)

air–water and planar oil–water interfaces (59), for hydrocarbon oil–water interfaces in emulsions (64), and for interfaces between water and polystyrene latex particles (65–67) and hydrophobized silica (68). At the triglyceride–water interface, however, the adsorbed amount is somewhat lower (69).

Information about the adsorbed layer structure of β-casein at the hydrophobic surface can be obtained by employing neutron reflectivity, small-angle x-ray scattering (SAXS), and dynamic light scattering. It was found that the layer of β-casein adsorbed to a hydrocarbon oil–water interface or an air–water interface (70,71) consisted of a dense inner part, 2 nm thick, and a protein volume fraction of 0.96, immediately adjacent to the interface. Beyond that, a second dilute region with a protein volume fraction of 0.15 extended into the aqueous phase. A similar structure of β-casein adsorbed onto polystyrene latex particles was observed with SAXS (65). The electron density profile calculated from the SAXS data indicated that most of the protein resided within 2 nm from the surface. The profile

also showed a small amount of protein extending some 10 nm into the aqueous phase. Further, the hydrodynamic layer thickness estimated from the diffusion coefficient determined by dynamic light scattering of latex particles (67,72,73) and emulsion droplets (69) coated with β-casein was found to be 10–15 nm. The fact that different experimental techniques give a different value of the layer thickness is simply because they have a different sensitivity to the extending tails.

This type of layer structure, with a compact inner region and a dilute outer region, was also predicted by self-consistent field theory and by computer simulations. For instance, Monte Carlo simulations show that a dense layer (1–2 nm thick) is present close to the planar interface (74). This layer contained about 70% of the segments. Further out, a region of much lower density was found to extend about 10 nm into the aqueous phase. Similar results were obtained by self-consistent field calculations (75), which also showed that the most hydrophilic segments reside predominantly in the outer layer.

The properties of adsorbed β-casein layers can be changed by the action of enzymes. Leaver and Dalgleish (69) have observed that the N-terminal end is more accessible to trypsinolysis than the rest of the adsorbed molecule, and that loss of the tail leads to a reduced layer thickness. A similar change was observed by Nylander and Wahlgren (68), who found that the addition of endoproteinase ASP-N to an adsorbed layer of β-casein reduced the adsorbed amount by approximately 20%. The removal of the extending tails will clearly reduce the range of the stabilizing steric force and thus reduce the emulsion stability against flocculation. We note that the forces generated by adsorbed β-casein are not very strongly repulsive (Fig. 14). Hence, the excellent stability of emulsion droplets coated by β-casein is most likely because the hole nucleation energy barrier is high.

Proteoheparan sulfate is an amphiphilic membrane glycoprotein. Like β-casein, it has one large hydrophobic region. Proteoheparan sulfate has three to four hydrophilic and strongly charged side chains, whereas β-casein has only one less charged tail. Protoheparan sulfate is not used for stabilizing emulsions. However, it is nevertheless of interest to compare the forces generated by this protein with those generated by β-casein. The interaction between hydrophobic surfaces across a 1-mM NaCl solution containing 0.2 mg proteoheparan sulfate/mL is shown in Fig. 14 (62,76). The long-range interaction is dominated by a repulsive double-layer force, considerably stronger than that observed for β-casein. This is simply because proteoheparan sulfate is more strongly charged than β-casein. A steric force dominates the short-range interaction for both proteins.

F. Phospholipids on Polar Surfaces in Oil

We have seen earlier that surface force measurements provide important information about interactions between solid hydrophobic surfaces coated with surfactants and polymers, and that some of the information obtained is directly relevant for oil-in-water emulsions. However, the details of the interaction profiles are expected to be different for liquid hydrocarbon droplets coated with the same molecules as the model solid surfaces. In particular, the coalescence behavior of the emulsion droplets cannot be modeled. It is even more difficult to make a solid model surface that mimicks the behavior of water-in-oil emulsions. At present, the best one can do is to use a polar surface that attracts the polar part of the emulsifier. In this way, the orientation of the emulsifier on the model surface and at the water-in-oil emulsion surface will be the same. This will allow us to draw some conclusions about how polar solid surfaces coated with emulsifiers interact across oil, but care should be taken when using such results to draw conclusions about water-in-oil emulsions.

The forces between polar mica surfaces interacting across triolein containing 200 ppm of soybean phosphatidylethanolamine (PE) have been studied (77). Some results obtained at two different water activities are illustrated in Fig. 15. When the water activity is 0.47, a monolayer of PE is adsorbed on each surface. The orientation is such that the polar group is attached to the mica surface with the nonpolar part directed toward the oil phase. Thus, adsorption of the phospholipid renders the mica surface nonpolar. No force is observed until the surfaces are about 6 nm apart. At this point, a very steep repulsion is experienced which is due to compression of the adsorbed layers. A weak attraction is measured on separation. The forces change significantly when the trioein is saturated with water (water activity = 1). The adsorbed layer becomes significantly thinner, and now only a rather weak compressive force is needed in order to merge the two adsorbed layers into one. The reason is that water molecules adsorb next to the polar mica surface and in the region of the zwitteronic lipid head group. This increases the mobility of the adsorbed phospholipid and decreases the force needed to merge the two adsorbed layers. Interestingly, it is not possible to remove the last adsorbed layer even by employing a very high compressive force.

From these observations, we can draw some conclusions that are relevant for water-in-oil emulsions. First, no long-range electrostatic forces are present in the nonpolar media. This is because the dissociation of surface groups is very unfavorable in low-polarity media. Hence, generally it is very difficult to utilize electrostatic forces for generating long-range stabilizing forces in oil. Surfactants like phospholipids or alkyl ethoxylates adsorbed

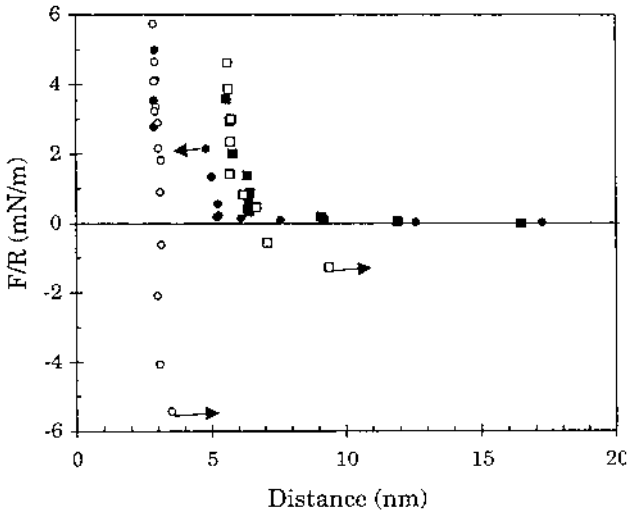

Figure 15 Force normalized by radius between mica surfaces in crossed cylinder geometry interacting across a triolein solution containing 200 ppm of soybean phosphatidylethanolamine. The forces of soybean were measured at water activities of 0.47 on approach (■) and separation (□), as well as at a water activity of 1 on approach (●) and separation (○); the arrows indicate inward and outward jumps. (From Ref. 77, with permission.)

in monolayers will only generate short-range repulsive forces due to compression of the hydrocarbon chains penetrating into the oil medium. These substances will be efficient in preventing coalescence of water-in-oil emulsions only when the adsorbed amount is high enough and the spontaneous monolayer curvature is sufficiently negative.

G. Polymers on Polar Surfaces in Oil

We saw earlier that surfactants adsorbed in monolayers only give rise to rather short-range forces in oil media. The range of the forces can be increased considerably if liquid-crystalline phases are accumulated at the interface, or if amphiphilic oil-soluble polymers are used instead of low-molecular-weight surfactants. An example of such a polymer is PGPR (polyglycerol polyricinoleate), which is a powerful water-in-oil emulsifier used in the food industry (78). PGPR has a complex branched structure as indicated in Fig. 16. This polymer was used for studying interactions between polar mica surfaces in triolein (79). The forces obtained at a polymer concentration of 200 ppm are shown in Fig. 17. In this system, repulsive steric forces are observed at distances below 15 nm. The magnitude of the

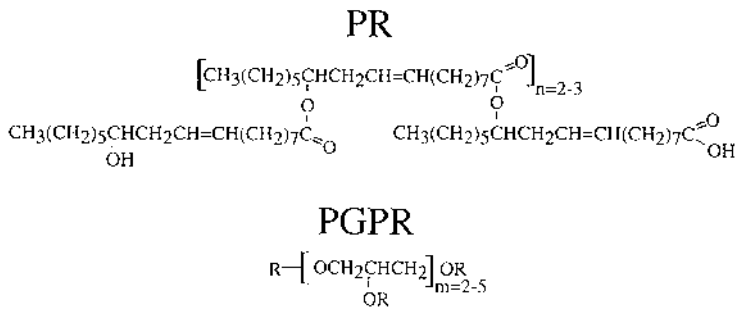

Figure 16 Illustration of the structural elements of PGPR. The upper structure is that of the polyricinoleate moiety; the lower structure shows the polyglycerol backbone. The R in the structure can be either hydrogen, a fatty acid residue, or a polyricinoleate residue. In PGPR, at least one of the side chains is polyricinoleate.

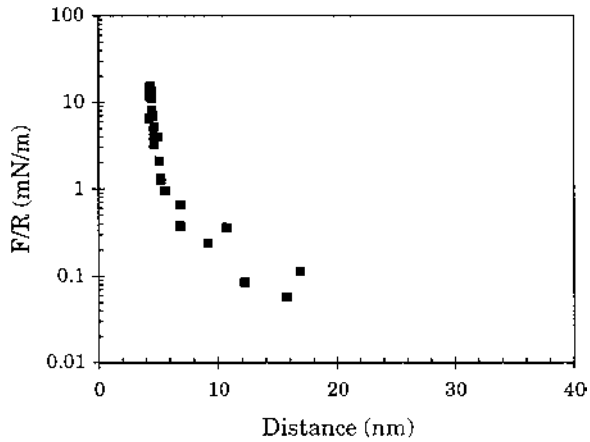

Figure 17 Force normalized by radius between mica surfaces interacting across a triolein solution containing 200 ppm of PGPR measured on approach.

force increases rather slowly with decreasing surface separation until the surfaces are about 5 nm apart. A further compression of the layers results in a steep increase of the steric force. The force profile indicates that the adsorbed layer consists of an inner dense region and an outer dilute region with some extended tails and loops. When dense polymer layers that generate long-range steric forces and have a high surface elasticity and viscosity are adsorbed at the interface of water-in-oil emulsions, one can expect that the emulsion stability against flocculation and coalescence will be good.

H. Forces Between Surfaces Across Emulsions

Emulsion droplets do not only break by coalescing with each other, but they may also break by attaching to a solid surface. Depending on the application, this may be wanted or unwanted. In order to study emulsion–surface interactions, a model oil-in-water emulsion was prepared from purified soybean oil (20 wt%) using fractionated egg phosphatides (1.2 wt%) as the emulsifier. The mayor components of the emulsifier were phosphatidylcholines and PEs. The mean diameter (D_Z average) of the emulsion was 320 nm, as determined with photon-correlation spectroscopy. A small amount of negatively charged lipids was also present, giving the emulsion droplets a net negative zeta potential of about −40 mV (80). This emulsion was then placed inside a SFA.

The forces acting between two glass surfaces across the 20% oil-in-water emulsion measured by using the MASIF are illustrated in Fig. 18 (81). A repulsive force dominates the interactions at separations below 200 nm.

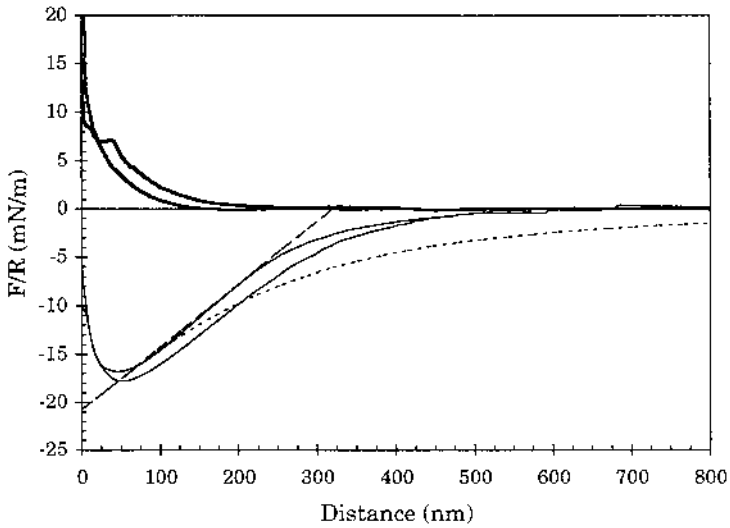

Figure 18 Force normalized by local geometric mean radius as a function of surface seperation between glass across a concentrated emulsion solution (20 wt% oil and 1.2 wt% phospholipid). The thinner lines correspond to the force measured on separation, the dashed line represents the calculated force between two spherical surfaces connected by a capillary condensate in the full equillibrium case [Eq. (25)], and the dotted line represents the force between two spherical surfaces connected by a capillary condensate in the nonequillibrium case [Eq. (26)]. (From Ref. 81, with permission.)

The force increases strongly with decreasing distance. This illustrates that large aggregates, with a diameter of at least 100 nm, are associated with each surface and the repulsion between 40 and 200 nm is due to deformation and eventual breaking of these aggregates. The range of the repulsive force is consistent with the layer thickness obtained in a previous ellipsometric study by Malmsten et al. (80). They found that the thickness of a layer adsorbed from the emulsion on to a negatively charged silica surface was around 100 nm, independent of surface coverage.

In some force curves, one or two distinct steps are present. Figure 18 illustrates one such force curve where a clear step is seen at a separation of about 40 nm. At a separation of about 10 nm, another step, but less pronounced, is seen. These steps are interpreted as being due to coalescence of adsorbed emulsion droplets and/or due to materials that collectively leave the zone between the surfaces. On subsequent approaches of the surfaces on the same position, the range of the repulsion remains at about 200 nm. However, the steps in the force profile become less pronounced or disappear completely, indicating a change in the adsorbed layer when exposed to a high compressive force.

A strong and long-range force is observed when the surfaces are separated. It is plausible that this attraction is due to the formation of a capillary condensate of oil between the surfaces (Fig. 19). This capillary condensate originates from the emulsion droplets that have been destroyed when the surfaces are brought together. The forces between two spherical surfaces connected by a capillary condensate in the full equilibrium case are given by (82)

$$\frac{F}{R} = 2\pi(\sigma_{sc} - \sigma_{sb})\left(1 - \frac{D}{R_k}\right) \tag{25}$$

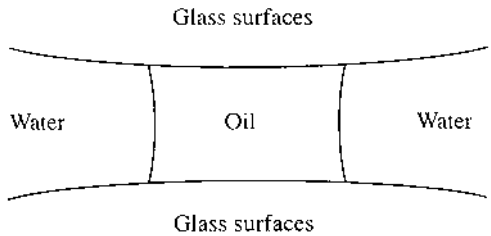

Figure 19 Schematic of the capillary condensate formed between glass surfaces due to breakdown of adsorbed emulsion droplets. The figure is not according to scale. (From Ref. 81, with permission.)

where σ is the interfacial tension and the subscript s, c, and b stand for surface, capillary condensate, and bulk, respectively; R_K is the Kelvin radius of the capillary condensate. In cases when the surfaces are separated too rapidly to allow the volume of the capillary to change with separation, one instead obtains (82)

$$\frac{F}{R} = 2\pi(\sigma_{sc} - \sigma_{sb})\left[1 - \frac{1}{\sqrt{(1 + R_k^2/D^2)}}\right] \tag{26}$$

Two theoretical force curves calculated by using Eqs. (25) and (26) are shown in Fig. 18. In these calculations, we used a Kelvin radius of 320 nm and an interfacial tension difference of 3.3 mN/m. The measured force curves fall in between the extreme cases of full equilibrium, where the volume of the condensate is changing with distance to minimize the free energy, and the case of no change in condensate volume with separation. Long-range forces due to capillary condensation have been observed previously by Petrov et al., who found that a lamellar phase condensed between two surfaces immersed in an L_3-phase (83). Capillary condensation of sparingly soluble surfactants between surfaces close to each other in surfactant solutions has also been reported (84).

It is worth pointing out that the functional form of the measured attraction shows that the volume of the capillary condensate decreases with increasing separation. However, this does not occur fast enough compared to the speed of the measurements (the attractive part took about 30 s to measure) to allow full equilibrium to be established. Also, the range of the measured repulsion on approach does not increase with the number of times the surfaces are brought into contact but rather the reverse. Both of these observations point to the fact that the material present in the capillary condensate is spontaneously reemulsified when the surfaces are separated.

In order to obtain information about whether a monolayer, a bilayer, or a multilayer was firmly attached to the surfaces, we employed the interferometric SFA and mica surfaces rather than glass surfaces (81). In these measurements, a drop of the emulsion was placed between the surfaces. The emulsion was very opaque and no interference fringes could be seen until the surfaces were close to contact. The force measured between mica surfaces across a concentrated emulsion were repulsive and long range (several hundred nanometers), which was in agreement with the results obtained using glass surfaces. Because the forces were so highly repulsive, no attempt was made to measure them accurately, but under a high compressive force, the

surfaces come to a separation 8.5 nm. This corresponded to a bilayer of phospholipid on each surface.

I. Forces Due to Stratification in Foam and Pseudoemulsion Films

The thinning of thin liquid films in micellar solution is found to occur in a stepwise fashion, known as stratification. Bergeron and Radke (35) set out to study the forces responsible for this phenomenon using the porous frit version of the thin-film pressure balance. They found that the equilibrium disjoining pressure curve (force curve) showed an oscillatory behavior both for foam and pseudoemulsion (i.e., asymmetric oil–water–gas) films stabilized by the anionic surfactant sodium dodecyl sulfate above the cmc (Fig. 20). The reason for this oscillatory force profile was the layering of micelles in the confined space in the thin aqueous film separating the two interfaces. The periodicity of the oscillations was the same for foam films and for pseudoemulsion films. The main difference between the two systems was found in the high-pressure region of the disjoining pressure isotherm. The pseudoemulsion films ruptured at much lower imposed pressures than the foam films. This was attributed to the action of the oil phase as a foam destabilizer.

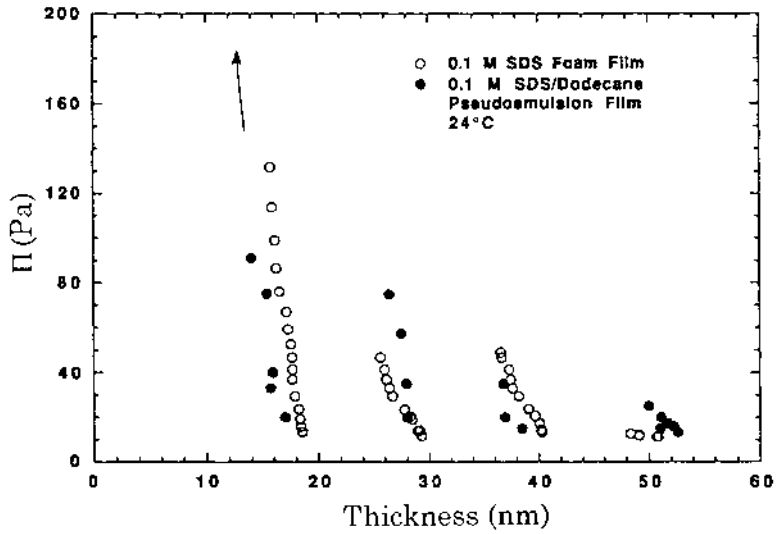

Figure 20 Low-pressure region of the disjoining pressure isotherm across a 0.1 M SDS solution in a single-foam lamella, and across a 0.1 M SDS solution separating a dodecane–solution interface from an air–solution interface. (Reproduced from Ref. 35, with permission.)

VI. SUMMARY

Several techniques are available for studying long-range interactions between solid surfaces and fluid interfaces. The forces generated by surfactants, polymers, and proteins have been determined. For oil-in-water emulsions, both steric and electrostatic stabilizing forces are of importance, whereas only steric forces are operative for the case of water-in-oil emulsions. These forces are well understood theoretically. The experimental techniques employed give very detailed information on the long-range forces, and in this respect, the results obtained for the model systems can be useful for understanding interactions in emulsion systems. However, the surface force techniques employed are not suitable for modeling the molecular events leading to coalescence of emulsion droplets once they have been brought in close proximity to each other. Some data illustrating the breakdown and reemulsification of emulsion droplets in the gap between two macroscopic solid surfaces were also presented. This is a new research topic and very little is known about how the surface properties and the type of emulsifier influence the stability of emulsion droplets at surfaces and in narrow gaps between surfaces.

ACKNOWLEDGMENT

This work was partly sponsored by the Competence Centre for Surfactants Based on Natural Products (SNAP).

REFERENCES

1. W. D. Bancroft, *J. Phys. Chem.* 19, 275 (1915).
2. W. C. Griffin, *J. Soc. Cosmet. Chem* 1, 311 (1949).
3. J. T. Davies, *Proc. 2nd Int. Congr. Surf. Activity* 1957, Vol. 1, 426.
4. A. Kabalnov and H.Wennerström, *Langmuir* 12, 276 (1996).
5. D. Y. C. Chan and R. G. Horn, *J. Chem, Phys.* 83, 5311 (1985).
6. J. Kizling and B. Kronberg, *Colloids Surfaces* 50, 131 (1990).
7. O. Reynolds, *Phi. Trans. R. Soc. London* 177, 157 (1886).
8. F. W. Cain and J. C. Lee, *J. Colloid Interf. Sci.* 106, 70 (1985).
9. E. D. Manev and R. Tsekov, and B. P. Radoev, *J. Dispers. Sci. Technol.* 18, 769 (1997).
10. B. P. Radoev, A. D. Scheludko, and E. D. Manev, *J. Colloid. Interf. Sci.* 95, 254 (1983).
11. S. A. K. Jeelani and S. Hartland, *J. Colloid Interf. Sci.* 164, 296 (1994).

12. J. N. Israelachvilli, *Intermolecular and Surface Forces,* Academic Press, London, 1991.
13. E. J. N. Verwey and J. T. G. Overbeek, *Theory of Stability of Lyophobic Colloids,* Elsevier, Amsterdam, 1948.
14. B. V. Derjaguin and L. Landau, *Acta Physicochim. URSS* 14, 633 (1941).
15. V. A. Parsegian, N. Fuller, and R. P. Rand, *Proc. Natl. Acad. Sci. USA* 76, 2750 (1979).
16. J. N. Israelachvili and H. Wennerström, *J. Phys. Chem.* 96, 520 (1992).
17. G. J. Fleer, M. A. Cohen Stuart, J. M. H. M. Scheutjens, T. Cosgrove, and B. Vincent, *Polymers at Interfaces,* Chapman & Hall, London, 1993.
18. P.-G. de Gennes, *Scaling Concepts in Polymer Physics*, Cornell University Press, Ithaca, NY, 1979.
19. P.-G. de Gennes, *Adv. Colloid Interf. Sci.* 27, 189, (1987).
20. A. D. Nikolov and D. T. Wasan, *J. Colloid Interf. Sci.* 133, 1–12, (1989).
21. V. Bergeron and C. J. Radke, *Langmuir* 8, 3020 (1992).
22. V. Bergeron, A. J. Jiménez-Laguna, and C. J. Radke, *Langmuir* 8, 3027 (1992).
23. V. Bergeron, Forces and structure in surfactant-laden thin-liquid films, PhD thesis, University of California, Berkeley, 1993.
24. A. L. de Vries, *Rec. Trav. Chim. Pays-Bas* 77, 383 (1958).
25. K. Shinoda and H. Saito, *J. Colloid Interf. Sci.* 30, 258 (1969).
26. P. M. Claesson, T. Ederth, V. Bergeron, and M. W. Rutland, *Adv. Colloid Interf. Sci.*67, 119 (1996).
27. J. N. Israelachvili, G. E. Adams, *J. Chem. Soc. Faradav Trans. I* 74, 975 (1978).
28. J. Parker, *Prog. Surf. Sci.* 47, 205 (1994).
29. K. Schillén, P. M. Claesson, M. Malmsten, P. Linse, and C. Booth, *J. Phys. Chem.* 101, 4238 (1997).
30. B. Derjaguin, *Kolloid Z.* 69, 1557 (1934).
31. R. G. Horn, J. N. Israelachvili, and F. Pribac, *J. Colloid Interf. Sci.* 115, 480 (1987).
32. P. Attard and I. L. Parker, *Phys. Rev. A* 46, 7959 (1992).
33. A. Scheludko, *Adv. Colloid Interf. Sci.* 1, 391 (1967).
34. O. D. Velev, G. N. Constantinides, D. G. Avraam, A. C. Paytakes, and R. P. Borwankar, *J. Colloid Interf. Sci.* 175, 68 (1995).
35. V. Bergeron and C. J. Radke, *Colloid Polym. Sci.* 273, 165 (1995).
36. K. J. Mysels and M. N. Jones, *Disc. Faraday Soc.* 42, 42 (1966).
37. R. L. Ferm, in *Emulsion and Emulsion Technology* (K. J. Lissant, ed.), Marcel Dekker, New York, 1974, Vol I p. 387.
38. V. Bergeron, *Langmuir* 13, 3474 (1997).
39. P. C. Herder, *J. Colloid Interf. Sci.* 134, 336 (1990).
40. P.M. Claesson, R. Kjellander, P. Stenius, and H. K. Christenson, *J. Chem. Soc. Faraday Trans. I* 82, 2735 (1986).
41. R. Kjellander, *J. Chem. Soc. Faraday Trans. II* 78, 2025 (1982).
42. R. E. Goldstein, *J. Chem. Phys.* 80, 5340 (1984).
43. G. Karlström, *J. Phys. Chem.* 89, 4962 (1985).
44. A. Matsuyama and F. Tanaka, *Phys. Rev. Lett.* 65, 341 (1990).

45. P.-G. de Gennes, *C.R. Acad. Sci. Paris* 313, 1117 (1991).
46. S. Bekiranov, R. Bruinsma, and P. Pincus, *Europhys. Lett.* 24, 183 (1993).
47. P. Linse and B. Björling, *Micromolecules* 24, 6700 (1991).
48. M. Björling, *Macromolecules* 25, 3956 (1992).
49. W. Brown, R. Johnsen, P. Stilbs, and B. Lindman, *J. Phys. Chem.* 87, 4548 (1983).
50. G. J. T. Tiddy, *Phys. Rep.* 57, 3 (1980).
51. D. J. Mitchell, G. J. T. Tiddy, L. Waring, T. Bostock, and M. P. McDonald, *J. Chem. Soc. Faraday Trans. I* 79, 975 (1983).
52. J. N. Israelachvili, D. J. Mitchell and B. W. Ninham, *J. Chem. Soc. Faraday Trans. II* 72, 1525 (1976).
53. S. I. Jeon and J. D. Andrade, *J. Colloid Interf. Sci.* 142, 159 (1991).
54. K. Shinoda and H. Takeda, *J. Colloid Interf. Sci.* 32, 642 (1970).
55. B. A. Bergenståhl and P. M. Claesson, in *Food Emulsions* (S. E. Friberg and K. Larsson, eds), Marcel Dekker, New York, 1997.
56. S. E. Friberg and C. Solans, *Langmuir* 2, 121 (1986).
57. G. F. Belder, Gten Brinke and G. Hadziioannou, *Langmuir* 13, 4102 (1997).
58. P. Fäldt, B Bergenståhl and P. M. Claesson, *Colloids Surfaces A* 71, 187 (1993).
59. D. G. Schmidt and T. A. J. Payens, *J. Colloid Interf. Sci.* 39, 655 (1972).
60. E. Dickinson, *J. Dairy Sci.* 80, 2607 (1997).
61. H. E. Swaisgood, *Development in Dairy chemistry— 1*, Applied Science, London, 1982.
62. P. M. Claesson, E. Blomberg, J. C. Fröberg, T. Nylander, and T. Arnebrandt, *Adv. Colloid Interf. Sci.* 57, 161 (1995)
63. T. Nylander and N. M. Wahlgren, *Langmuir* 10, 1274 (1997).
64. J.-L. Courthaudon, E. Dickinson, and D. G. Dalgleish, *J. Colloid Interf. Sci.* 145, 390 (1991).
65. A. R. Mackie, J. Mingins, and A. N. North, *J. Chem. Soc. Faraday Trans.* 87, 3043 (1991).
66. J. R. Hunter, P. K. Kilpatrick, and R. G. Carbonell, *J. Colloid Interf. Sci.* 142, 429 (1991).
67. D. V. Brooksbank, C. M. Davidson, D. S. Horne, and J. Leaver, *J. Chem. Soc. Faraday Trans.* 89, 3419 (1993).
68. T. Nylander and N. M. Wahlgren, *J. Colloid Interf. Sci.* 162, 151 (1994).
69. J. Leaver and D.G. Dalgleish, *J. Colloid Interf. Sci.* 149, 49 (1992).
70. E. Dickinson, *J. Chem. Soc. Faraday Trans.* 88, 2973 (1992).
71. E. Dickinson, D. S. Horne, J. S. Phipps, and R. M. Richardson, *Langmuir* 9, 242 (1993).
72. D. G. Dalgeish, *Colloids Surfaces* 46, 141 (1990).
73. D. G. Dalgleish and J. Leaver, *J. Colloid Interf. Sci.*141, 288 (1991).
74. E. Dickinson and S. R. Euston, *Adv. Colloid Interf. Sci.* 42, 89 (1992).
75. F A. M. Leermakers, P. J. Atkinson, E. Dickinsin, and D. S. Horne, *J. Colloid Interf. Sci.* 178, 681 (1996).
76. M. Malmsten, P. M. Claesson, and G. Siegel, *Langmuir* 10, 1274 (1994).
77. A. Dedinaite, P. M. Claesson, B, Campbell, and H. Mays. *Langmuir* 14, 5546 (1998).

78. R. Wilson, B. I. van Schie, and D. Howes, *Food Chem. Toxicol*. 36, 711 (1998).
79. A. Dedinaite, B. Campbell, *Langmuir* 16, 2248–2253 (2000).
80. M. Malmsten, A.-L. Lindström, and T. Wärnheim, *J. Colloid Interf. Sci*. 173, 297 (1995).
81. E. Blomberg, P. M. Claesson, and T. Wärnheim, *Colloids Surfaces A,* 159, 149–157 (1999).
82. D. F. Evans and H. Wennerström, *The Colloidal Domain,* 2nd ed., VCH, New York, 1998.
83. P. Petrov, U. Olsson, and H. Wennerström, *Lanfmuir* 13, 1000, (1979).
84. Å. Waltermo, P. M. Claesson, and I. Johansson, *J. Colloid Interf. Sci*. 183, 506 (1996).